HHS Public Access

Author manuscript

IEEE Trans Biomed Eng. Author manuscript; available in PMC 2018 July 01.

Published in final edited form as:

IEEE Trans Biomed Eng. 2018 July ; 65(7): 1468–1475. doi:10.1109/TBME.2017.2749245.

Unambiguous Identification and Visualization of an Acoustically Active Catheter by Ultrasound Imaging in Real Time: Theory, Algorithm, and Phantom Experiments

Viksit Kumar [Member, IEEE],
Department of Physiology and Biomedical Engineering, Mayo Clinic, Rochester, MN, USA

Richard Liu,
Department of Physiology and Biomedical Engineering, Mayo Clinic, Rochester, MN, USA

Randall R. Kinnick,
Department of Physiology and Biomedical Engineering, Mayo Clinic, Rochester, MN, USA

Adriana Gregory [Member, IEEE],
Department of Radiology, Mayo Clinic, Rochester, MN, USA

Azra Alizad [Senior Member, IEEE],
Department of Radiology, Mayo Clinic, Rochester, MN, USA

Marek Belohlavek, and
Department of Cardiovascular Diseases, Mayo Clinic, Scottsdale, AZ, USA

Mostafa Fatemi [Fellow IEEE]
Department of Physiology and Biomedical Engineering, Mayo Clinic, Rochester, MN, USA

Abstract

Objective—Ultrasound-guided biopsies and minimally invasive procedures have been used in numerous medical applications, including catheter guidance. The biggest challenge for catheter guidance by ultrasound lies in distinguishing the catheter from neighboring tissue, as well as the ability to differentiate the catheter body from its tip.

Methods—In our previous work, we introduced a functional prototype of an acoustically active catheter, in which a miniature piezoelectric crystal allowed accurate localization of the catheter tip by pulsed wave (PW) Doppler imaging and Doppler spectrogram. In the current paper, the theory behind the symmetric Doppler shift due to the interaction of ultrasound wave with a vibrating piezoelectric crystal is explained. The theory is validated in an experimental continuous flow phantom setup. A novel algorithm, Symmetric frequency detection (SFD) algorithm is presented for identification and visualization of the catheter tip in real time along with B-mode and PW Doppler.

Correspondence to: Mostafa Fatemi.
Richard Liu is currently with the Department of Biomedical Engineering, Johns Hopkins, Baltimore, MD, USA.

Results—The catheter tip is identified with a distinct color differentiable from common Doppler colors with a frame rate varying from 22 to 50 Hz. The catheter tip can be visualized in a small region of 2.4 mm in the elevational direction.

Conclusion—The algorithm can be implemented in most clinical ultrasound machines with minor additions to the PW Doppler processing algorithm. The algorithm is optimized to be robust for a variety of blood flow velocities and is shown to perform well when the signal from the blood is on par in amplitude with the catheter signal.

Significance—Unambiguous and distinct visualization of catheter tip facilitates real-time tracking of the catheter tip aids minimally invasive procedures.

Keywords

acoustic; catheter; Doppler; navigation; real-time; ultrasound guidance; vibration

INTRODUCTION

Minimally invasive procedures are rapidly replacing conventional invasive surgery due to smaller incisions, less scar tissue, lower risk of infection, shorter hospitalization, and faster recovery time. Ultrasound imaging has been used for guidance of minimally invasive procedures for years and has advanced by employing 3D cardiac ultrasound for guiding deployment of valve prostheses [1] and closure devices [2, 3].

Despite these advances, the fundamental limitations of sound propagation and ultrasound image artifacts impede guidance and exact targeting of catheters for investigative (electrophysiology), diagnostic (biopsy), or therapeutic (drug delivery of cellular or molecular therapy) purposes. Conventional invasive devices are difficult to locate with conventional pulse echo ultrasound due to the specular nature of the invasive device. In order to better visualize the invasive device, hyperechoic needles with a screw have been used to increase the number of reflective surfaces [4]. However that does not aid in identifying the tip of the needle and improvement in visualization is also limited.

Angiography and other fluoroscopic techniques provide planar projection of complex 3D organs with limited visualization of anatomy. The key benefit of the proposed nonionizing guidance by ultrasound is in navigating the catheter along with real-time depiction of its surrounding anatomy. Additional benefits include simultaneous Doppler analysis of blood flow through vasculature, cardiac cavities, and valves, as well as portability, cost effectiveness, and wide availability. Due to fundamental limitations of ultrasound imaging, we anticipate complementary role of ultrasound navigation to fluoroscopy. Transesophageal ultrasound navigation of transcutaneous aortic valve replacement and blood flow analysis during and immediately after the procedure is a good example of this growing trend.”

Nevertheless, ultrasound guidance methods can also have inherent problems. For example, the catheter tip can be confused with other parts of the catheter shaft within an ultrasound image plane. The catheter could also have the same level of brightness as the surrounding anatomy, i.e., ultrasonography does not resolve all possible image ambiguities arising from

the B-mode image. Some of the uncertainty between identification of catheter versus anatomy can be overcome by controlled movement of the catheter by the user.

In our previous work [5], we developed and initially tested a prototype of an acoustically active tip catheter, intended primarily for intracardiac guidance. A miniature crystal was placed at the tip of a catheter to act as a "beacon" that allowed unique and accurate localization of the catheter tip by pulsed-wave (PW) Doppler imaging. Unlike approaches used by others, which require substantial modification of the ultrasound imaging system hardware [6] or use of a complex external magnetic navigation assembly [7-9], our method does not require any modification to the ultrasound imager, and any ultrasound system capable of PW Doppler imaging could be used. The PW Doppler navigation method can localize the catheter tip within a few millimeters of a point target [5]. Previous work by [10] describes the use of a passive detector to identify the catheter tip and mark the location in the image with an arrow. Yet another investigation team vibrated the whole aspiration needle at high frequency and low amplitude [11] for better localization of the needle tip using color Doppler. However, in contrast to those techniques, our method uses an active acoustic point source on the tip of the catheter, which provides a much smaller target, thus allowing for better localization of the source of vibration. *Reddy et al.* (2008) used a motor rotating at 11,000 rpm attached to the proximal end of the cardiac electrophysiologic catheter that could be visualized in the Doppler mode, but the Doppler image suffered from severe artifacts.

In the current study, we present the basic physical theory of Doppler shifts produced by interactions of the vibrating piezoelectric crystal and the incident ultrasound signal. We introduce an algorithm that can be used to visualize the catheter tip using a distinct color scheme in PW Doppler imaging setup. We also present the implementation of the algorithm in a real-time ultrasound research system and validate it with a continuous flow phantom.

MATERIALS AND METHODS

A. Theory of Harmonic Generation

The physics behind the scattering of ultrasound waves with a vibrating surface have been studied previously [12-17]. An incident ultrasound pulse-echo wave with center frequency (f_c) scattered by a surface vibrating at a frequency (F_s) results in a scattered wave containing frequency components ($f_c \pm nF_s$), where n is an integer. The change in the frequency component of the scattered wave is due to the Doppler shift and acoustic nonlinearities in the bulk of the fluid [15, 16]. The prevalence of one phenomenon over the other (i.e., Doppler vs. nonlinearity) is determined by factors such as vibration amplitude, low frequency pressure, or distance between vibrating surface and receiving transducer. Irrespective of the phenomenon, both lead to spectral sidebands around the center frequency, i.e., $f_c \pm nF_s$ [15, 16]. The effect of bulk nonlinearities are negligible compared to the Doppler shift when the scattering happens in water or soft tissue, as opposed to air. In water, the Doppler effect is more dominant at higher frequencies (f_c in MHz range), whereas in air it is more dominant at lower frequencies [15, 16]. The effect of bulk nonlinearities increases as the distance between vibrating surface and receiving transducer increases, but is negligible close to the vibrating surface [15, 16]. In addition, F_s is fairly low (few kHz) compared to f_c (few MHz),

and its wavelength is long compared to the typical distance between the probe and the catheter. Based on the above considerations, it can be concluded that Doppler shift dominates bulk nonlinearity effects for the conditions in this paper. For consistency with our previous work [5], we will refer to the spectral sidebands as the *Doppler shift* throughout this paper.

Here, we briefly summarize the Doppler shift in the incident wave with frequency (f_c) due to modulation by a vibrating surface with frequency (F_s) [17]. Following the aforementioned argument, the nonlinear bulk effects are ignored for the purpose of derivation. The instantaneous angular frequency ω_i (t) of a wave reflected from a vibrating surface is approximated as:

$$\omega_i(t) = \omega_c + \Delta\omega\cos(\omega_s t), \quad (1)$$

, where $\omega_c = 2\pi f_c$ is the center angular frequency, $\omega_s = 2\pi F_s$ is the frequency of the vibrating surface, and $\Delta\omega$ is the peak frequency deviation value. The largest swing in frequency around the center frequency is indicated by ω_c. Because the instantaneous phase $\theta(t)$ is the time integral of the instantaneous angular frequency $\omega_i(t)$, then:

$$\theta(t) = \omega_c t + (\Delta\omega/\omega_s)\sin(\omega_s t) \quad (2)$$

Defining the modulation index $b = \Delta\omega/\omega_c$, Equation 2 can be rewritten as:

$$\theta(t) = \omega_c t + b\sin(\omega_s t) \quad (3)$$

Since the wave phase $\theta(t) = \omega_i t$, the equation of the reflected wave can be rewritten in complex form as

$$y(t) = \mathrm{Re}\left\{Ae^{j\theta(t)}\right\} = \mathrm{Re}\left\{Ae^{j(\omega_c t + b\sin(\omega_s t))}\right\} = \mathrm{Re}\left\{Ae^{j\omega_c t}e^{jb\sin(\omega_s t)}\right\}, \quad (4)$$

, where A is the amplitude of the ultrasound signal and Re{} denotes the real part of the complex quantity.

Since $e^{jb\sin(\omega_s t)} = \sum_{n=-\infty}^{\infty} J_n(b)e^{jn\omega_s t}$, where $J_n(\cdot)$ is the n-th order Bessel function of first kind, Equation 4 becomes:

$$y(t) = \mathrm{Re}\left\{A\sum_{n=-\infty}^{\infty} J_n(b)e^{j(\omega_c + n\omega_s)t}\right\} \quad (5)$$

The frequency spectrum of y(t) is obtained by taking the Fourier transform of this signal. Hence, the Fourier transform of Equation 5 is given as:

$$Y(\omega) = \mathrm{A}\pi \sum_{n=-\infty}^{\infty} J_n(b)\left[\delta(\omega - (\omega_c + n\omega_s)) + \delta(\omega + (\omega_c + n\omega_s))\right], \quad (6)$$

where $\delta(\cdot)$ is the Dirac delta function. Thus, the frequency spectrum $Y(\omega)$ has peaks at angular frequencies $\omega_c \pm n\omega_s$, where n is an integer. Since $\omega_c = 2\pi f_c$, the peaks will be found at frequencies $f_c \pm nF_s$.

B. Experimental Setup

The experimental setup in Figure 1 was used to measure the Doppler shift in the reflected pulse-echo signal due to a vibrating piezoelectric crystal. A custom-made gelatin phantom (12% gelatin by weight, 5% glycerol, 1% cellulose 20 μm, and 0.7% Laponite mixed into 800 mL of water) was set in a Plexiglas mold with damping material placed at the bottom to reduce reflected signals. While the gelatin phantom was setting, the base of the mold was angled at 30° so that a perpendicular insonification from the surface of the phantom would have a 60° incident angle to the flowing scatterers in the flow channel. This was considered the maximum recommended incident angle for Doppler ultrasound imaging [18]. A horizontal, cylindrical hole with diameter of 18 mm was bored into the gelatin phantom to allow for passage of blood-mimicking fluid. The cylindrical hole was designed to approximate aortic flow and surrounding tissues. A variable-speed continuous flow pump (Barnant Company, Barrington, IL, USA) delivered a blood-mimicking fluid (75% water, 25% glycerol with 6% cellulose 20 μm) from a reservoir, through the phantom hole, and into a secondary collection reservoir. A single-element piezoelectric crystal was bonded to a steel cardiac guide wire (with a diameter of 0.94 mm) using heat shrink wrap and passed downstream through a Y-junction with a stopper to minimize leakage. This wire was then adjusted manually to position the catheter tip in the desired location inside the artery-mimicking channel. The single-element piezoelectric crystal is made of Lead Zirconate Titanate (PZT-5H) and is shaped as a cylinder with a length and width of 1.27 mm and wall thickness of 0.25 mm. The piezoelectric crystal is covered in epoxy and has no backing material or matching layer.

A function generator (Model 33120A, Agilent Technologies, Inc., Santa Clara, CA, USA) produced a sinusoidal continuous-wave signal at 3 kHz, 3 mV peak-to-peak, and was the master trigger. The Crown Amplifier (Model XLS 202, Crown Audio, Inc., Elkhart, IN, USA) amplified the low frequency signal by 20 dB and excited the 2-mm diameter piezoelectric crystal (Sonometrics Corporation, London, ON, Canada). A linear array transducer L7-4 (Philips Healthcare, Andover, MA, USA) with a center frequency of 5 MHz was used for plane-wave imaging at a pulse repetition frequency (PRF) of 8 kHz using the Verasonics V-1 system (Verasonics Inc., Redmond, WA, USA). The Verasonics machine has two Intel Xeon X5650 processors with six cores, each running at 2.67 GHz; the system ram was 64 GB. The probe was positioned orthogonally to the surface of the phantom hole and clamped in position. In-phase Quadrature (IQ) data collected from the Verasonics machine was processed in real time using Matlab (The MathWorks Inc., Natick, MA, USA).

C. Algorithm

An ensemble of 32 frames was considered for processing each Doppler image. A projection initialization clutter filter was used to high-pass filter,(cut-off frequency is 100Hz), the signal to remove unwanted harmonics, potentially resulting in aliasing as well as low frequency signals from tissue movement. Fast Fourier transform (FFT) of the Doppler signal was taken through each point in space.

The processing steps described up to this point are similar to conventional Doppler processing algorithms; the additional steps required for identifying the catheter tip are described below. Any spatial point representing the catheter tip will have a Doppler shift in the neighborhood of catheter frequency. Since the signal from the catheter can be weak compared to the signal from the neighboring tissue, it was essential to estimate the signal and noise strength around the catheter frequency. A Gaussian window centered at a frequency of the catheter tip and standard deviation of 5% of the catheter frequency was used to extract the signal around the catheter frequency. Two rectangular windows were used to estimate the noise strength from other frequencies around the catheter frequency, but excluded the Gaussian window, which was used for signal strength. A threshold parameter α was defined as the ratio of signal power at catheter frequency to noise power in the neighborhood of the catheter. All spatial points satisfying the threshold requirement and within the frequency range of the catheter tip were passed through an adjacency filter. The adjacency filter was used to remove all connected components that had fewer than six pixels. The above-mentioned process was applied to all points in both the positive and negative Doppler shift frequencies. All spatial points satisfying the signal-to-noise threshold criteria for both positive and negative shift and adjacency filter were classified as the catheter tip. The identified pixels could then be overlaid on B-mode or Doppler images after passing through a Gaussian smoothing filter with a standard deviation of 0.6 and a kernel of size 0.62 mm in axial direction and 0.60 mm in lateral direction. A new binary color map with yellow color, which is distinct from the conventional red-blue Doppler color, is suggested to display the tip. Figure 2 summarizes the process as a flowchart.

The signal-to-noise threshold cutoff is dependent on the flow velocity, as the Doppler shift can cause an increase in signal strength at different frequencies. To find the minimum threshold cutoff value, two cases covering all velocities and then just high velocities are investigated. The threshold cutoff α is varied in steps of 0.5. Velocity cutoff is defined as the maximum blood flow velocity that needs to be observed in a given scenario. The velocity cutoff is varied in steps of 0.1 m/s. The location of the catheter tip is predicted using the above-mentioned algorithm and then comparing it with the manually marked position of the catheter tip on the B-mode image. The Sørensen-Dice index is used to measure the accuracy of the predicted catheter tip points. The Sørensen-Dice index for two sets, X and Y, can be calculated using Equation 7.

$$\text{Sørensen} - \text{Dice index} = \frac{2|X \cap Y|}{|X| + |Y|} \quad (7)$$

The algorithm detects symmetric Doppler shift and is named as Symmetric frequency detection (SFD) algorithm.

D. Choosing the Vibration Frequency of the Crystal

In order to detect a signal from the vibrating piezoelectric crystal using an ultrasound scanner, the vibration frequency (F_s) of the crystal should be chosen such that at least one pair of the resulting Doppler components falls within the Doppler bandwidth of the ultrasound scanner.

According to Doppler theory, the Doppler frequency shift (F_d) in the signal reflected from a source moving at a velocity (v) can be calculated as $F_d = 2f_c v\cos(\varphi)/c$, where f_c is the ultrasound transmit frequency, φ is the incident angle, and c is the ultrasound speed in the medium, approximately 1,480 m/s for water and 1,540 m/s for most tissues.

Clinical ultrasound scanners are designed to show flow velocity within a certain range. Let us assume that the maximum velocity that the system can show is v_{max}; then, the maximum Doppler frequency shift (F_{dmax}) is $F_{dmax} = 2f_c v_{maxc}os(\varphi)/c$. Therefore, by choosing F_s such that $nF_s < F_{dmax}$, we would be able to observe at least 2n Doppler components (both positive and negative Doppler shifts) of the crystal with the scanner system. For the purpose of this study, we chose a catheter frequency of 3 kHz to visualize both the positive and negative shift; a maximum frequency of 4 kHz is sufficient and implies a Nyquist criterion of 8 kHz for the sampling frequency. To make the FFT more efficient, an ensemble length of 32 was used so that the sample length is a multiple of 2. The frequency resolution can be given as $\Delta f = \frac{PRF}{el'}$, where el' is the modified ensemble length rounded up to the next power of 2 and PRF is the pulse repetition frequency of the ultrasound probe. In order to have a frequency component at the catheter excitation frequency, the catheter should be excited at frequencies as given by the formulation

$$f_{cath} = \left(\frac{e1'}{2} - N\right) * \Delta f; N \in Z^+, \frac{e1'}{2} > N > 1 \quad (8)$$

E. Localization Accuracy

In addition to visualizing the catheter tip, it is crucial to know the distance within which the catheter tip can be spatially localized. Localization distance is defined as the spot size that the piezoelectric crystal occupies in B-mode when vibrating. A short localization distance implies more accurate spatial tracking of the catheter tip. The localization distance depends on the scanning transducer and the piezoelectric crystal at the catheter tip. The piezoelectric crystal is spherical in shape and is omnidirectional. The localization distance in the azimuthal scanning direction will depend on the ultrasound beam width (BW) and the crystal size. However, in the axial direction, the localization accuracy will depend on the axial resolution of the linear array transducer and the crystal size. The axial resolution is usually submillimeter for both conventional and plane wave B-mode images. In the axial direction, the signal-to-noise ratio depends on the axial depth. As long as the signal strength from both components of the catheter is greater than the threshold α, the algorithm should

be able to identify the catheter tip. Elevational direction is the most important factor in localizing the catheter tip. Theoretically, the localization distance in elevational direction would depend on the ultrasound slice thickness (ST) and the size of the piezoelectric crystal (D_c). It would also depend on the noise and dynamic range, but those topics are beyond the scope of this work. As long as the crystal is within the ST of the ultrasound imaging plane, Doppler shifts are generated and thus can be detected by the Doppler system. However, if the crystal moves away from the beam, the amplitude of the ultrasound signal reflected by the crystal decays. Hence, the Doppler shift due to the crystal can no longer be detected. Therefore, the localization distance in the elevational direction is defined as

$$L_e = \frac{ST}{2} + D_c \quad (9)$$

To experimentally determine the localization accuracy in elevational direction, the piezoelectric crystal was suspended in a water tank and the linear array transducer was initially positioned 2-mm away from the center of the suspended crystal. The linear array was moved in the elevational direction for 4.2 mm in steps of 0.3 mm. Figure 3 shows the experimental setup in the water tank.

RESULTS

Figure 4 displays the spectral power density for a representative Doppler signal when the catheter tip lies in the ultrasound plane. The two peaks at ±3 kHz represent the symmetric Doppler shift due to the catheter tip, whereas the peak around 500 Hz is due to the flow of blood mimicking fluid in the flow phantom.

Figure 5 depicts the Gaussian-weighted window around the catheter tip signal along with the rectangular window for the noise estimation in the signal. The catheter tip signal is 8 dB lower than the blood flow signal in both Figures 4 and 5, and the noise floor is around –24 dB. In real-life scenarios, the blood flow signal is 40 to 100 dB lower than the surrounding tissue. The blood flow signal intensity is maintained high, by increasing scatterer concentration in blood-mimicking fluid, to evaluate the robustness of the algorithm in such a challenging setting. Figure 4 shows both positive and negative shifts in blood flow, suggesting some turbulence as the blood flow was unidirectional. Both the spectrums are shown after passing through a clutter filter.

To ensure the signal at catheter frequency originates from the catheter tip, a threshold cutoff for the signal is set based on the neighborhood noise level. The minimum threshold (α) can be suggested for different flow velocities, which would be particularly important in cases of high blood flow velocity, since the high velocity blood flow signal will start interfering with the catheter signal as the respective Doppler frequency shifts overlap. Figure 6(a) presents the result for minimum threshold selection for velocity cases from 10 to 90 cm/s. The 3D plot shows the blood flow velocity in X direction, α in Y direction, and Sørensen-Dice similarity coefficient (also represented as the color bar) in Z direction. The figure suggests the minimum threshold value for a given velocity cutoff. Similarly, Figure 6(b) represents the minimum threshold cutoff result for high-velocity cases ranging from 50 to 90 cm/s.

The above-mentioned algorithm was implemented on a research ultrasound platform from Verasonics. The visualization of the catheter tip can be conducted by two different modes. The first mode shows one window each for Doppler mode and catheter tip, as shown in Figure 7(a, b). The second mode shows the integrated display combining B-mode, Doppler, and catheter tip (represented in yellow), as seen in Figure 7(c). Reversing the direction of blood flow with an integrated display is shown in Figure 7(d). A frame rate of 22 Hz was obtained using two separate displays, whereas a frame rate of 15 Hz was obtained using a single integrated display. The difference in the frame rate is due to the custom code for the overlaying of three different maps on a single image, as the research machine was limited to overlaying two maps only. The frame rate is also affected by the size of the region of interest used for Doppler and catheter tip processing. The frame rate for the two separate displays increased from 22 to 50 Hz, when the region of interest size was decreased from 30 to 10 cm^2. The supplemental section shows a video S1 of the integrated display with the catheter moving in the elevational plane. The catheter tip is represented using a binary yellow color map. The catheter moves in and out of the imaging plane.

Figure 8 represents the changes in the first Doppler sideband amplitude due to elevational motion from –2 to 2.2 mm in steps of 0.3 mm. The –3 dB localization distance is 2.4 mm, which is just 0.4 mm larger than the crystal size. The amplitude falls by another 6 dB within 0.9 mm from the right edge of the –3 dB band.

DISCUSSION

We have developed a catheter with a tip that is acoustically active, unambiguously identified by PW Doppler, and can be displayed along with B-mode and Doppler images in real time with a frame rate as high as 22 Hz. The algorithm is a facile addition to the PW Doppler processing code and could be easily implemented in most clinical ultrasound machines. This novel use of PW Doppler is intended for guidance of minimally invasive procedures by ultrasound imaging.

Navigating the catheter tip by conventional B-mode imaging requires constant within-plane monitoring of the tip to avoid misrecognizing ultrasound projection through the catheter shaft as the catheter tip. In this paper, we present the theory behind the phenomenon of symmetric Doppler shift along with a novel algorithm to uniquely and unambiguously identify the catheter tip in the Doppler color flow image. The algorithm is validated using a flow phantom, and the localization accuracy of the catheter tip using this algorithm is tested in a water tank.

The initial method described in our previous study [5], in which a piezoelectric crystal placed at the catheter tip was uniquely identified within the small area of a PW Doppler sample volume, overcame the problem of mistaking the catheter shaft for its tip. Our previous study fell short, however, of depicting the catheter tip with a different color and required interactive manipulation with the PW Doppler sample volume. The currently proposed algorithm gets rid of the need of selecting a sample volume in the suspected catheter tip region for confirmation and, rather, directly overlays the vibrating crystal with a unique color, thus clearly indicating the catheter tip. The ability of the proposed algorithm to

detect the catheter tip in real time makes it convenient for the sonographer to quickly identify it.

Throughout testing, two distinct flow regimes were studied, each having a unique effect on spectral information. In lower-flow velocity cases, the peak signal power of the flow Doppler shift was considerably less than that of the power of the active tip, and also exhibited a smaller frequency spread due to a low flow velocity. The combination of having numerous points to estimate noise floor level and the lack of broadband noise resulted in a robust performance. However, in cases where peak flow velocity was increased beyond 60 to 70 cm/s, the spectral power of the Doppler shift signal exceeded that of the active tip and had a large frequency spread, which increased the broadband noise. Broadband noise limits the range of frequency from which the noise floor estimate may be estimated, resulting in an increased number of false negatives, as thresholding is done relative to the noise floor. The flow characteristics of the very high velocity cases suggest turbulent flow and potential introduction of air particles into the system, causing a Doppler shift signal far greater than what we would observe in a biological environment. However, this environment was included when suggesting the minimum threshold value for α to ensure that the algorithm was robust to such extreme conditions.

For high-velocity blood flow cases like atherosclerotic plaques, the blood flow Doppler shift can overlap with the Doppler shift from the vibrating crystal frequency. In such cases, the algorithm retains its ability to identify the catheter tip as the Doppler shift from the turbulent flow will not be symmetric to the blood Doppler shift. Whereas, the Doppler shift due to the catheter tip is a symmetric pair of Doppler shifts. The most challenging type of case is when the blood flow Doppler shift lies very close to, but does not exactly match, the vibrating crystal frequency. This causes the noise floor estimate to rise, and, as a result, the signal-to-noise ratio of the catheter tip may not pass the suggested threshold. Solutions to this problem include increasing the crystal frequency, amplitude, or both. However, the crystal frequency cannot be further increased if the Doppler PRF is already close to its maximum limit. Also, the driving signal amplitude to the crystal cannot be increased if there is a concern about thermal overheating of the catheter tip and voltage limitations for in-vivo applications.

The selection of frequencies to be used for estimating noise floor is crucial for the algorithm. For the proposed algorithm the noise floor is estimated from frequencies within the cutoff range (-100 to 100 Hz) of the high pass filter and the frequencies which lie beyond the maximum Doppler shift occurring from blood flow. Doppler shift from blood flow velocities rarely exceeds 3 kHz; exemptions can be made for pathological conditions like atherosclerotic plaques. Hence, frequencies beyond ±3 kHz can also be used for estimating noise floor. However, in cases of high blood flow velocity where the frequencies beyond 3 kHz are not available for estimating noise floor, other algorithms like MUSIC can be explored to estimate the frequency of the signal by modeling the signal to be compromised of two components: Blood flow shift, symmetric Doppler shift.

To find the minimum value of α, the process was repeated over all velocities and then just over high-flow velocities. Performance initially seems robust for a large range of α and velocity values, as seen in Figure 6(a), achieving a maximum average Sørensen-Dice

coefficient exceeding 0.6 with all velocities and low α cutoff. Low α cutoffs increase false positives throughout the image, but this does not reduce performance due to the adjacency filter, which ensures that only adjacent bulks of identified points are kept. The continuity of the catheter tip enables the use of an adjacency filter. However, the merits of low α cutoff are most evident in the high velocity test cases, where peak flow velocity for the same samples exceeds 50 cm/s and broadband noise is introduced. The falloff observed at higher α cutoffs and lower velocity cutoffs was only subtly visible in the 0 to 90 cm/s sample, but is dramatically more prominent in the 50 to 90 cm/s flow sample, as seen in Figure 6(b). Thus, the value of α used for further testing was 2.2 for a maximum speed of 85 cm/s. Different minimal values of α are anticipated for different clinical applications.

Unlike a real heart, the phantom used in these experiments has no bulk motion, which devoids the image of any tissue motion that can be a substantial source of noise in cardiac applications. This cardiac motion, however, does not have a symmetric frequency component, which makes it easier to discard these tissue motions in the frequency domain. The concentration of cellulose in blood-mimicking fluid is approximately 6%, whereas standard use is closer to 1% cellulose. This high concentration of cellulose increases the scattering strength of the blood-mimicking flow due to the high number of scatterers. Typically, the tissue signal is 40 to 100 dB higher than blood. This results in the blood signal being comparable to the vibrating crystal signal, thus making it even harder to differentiate the catheter tip from the blood. This challenging setting was used intentionally to scrutinize the robustness of the algorithm. Calculating the crystal signal strength relative to its surrounding frequencies and checking for symmetric frequency components ensures that the catheter tip can be distinguished even in the noisiest conditions.

The results shown in Figure 8 are important for clinical implications. The catheter has a small localization distance, implying that it can only be detected in a narrow region in the elevational direction of the imaging plane. The localization distance is greater than the size of the crystal due to the interference of the crystal field and the slice thickness in the linear-array transducer. The decrease in amplitude to –9 dB at a distance of 0.9 mm from the localization further helps in narrowing the localization distance of the catheter tip. This pragmatically enables the tip could be accurately guided along the axial direction of a given ultrasound beam within a 2D scan plane.

A. Conventional vs Plane Wave Machines

The above-mentioned algorithm was implemented using an ultrasound platform that has the capability of performing plane wave imaging. The ability to perform plane wave imaging provides a higher frame rate, which enables larger Doppler ensemble lengths and better frequency resolution. In a conventional ultrasound system with line-by-line beamforming, the Doppler ensemble length is usually between 16 and 20. The proposed algorithm can be used in a conventional ultrasound machine by reducing the Doppler pulse repetition frequency, the Doppler ensemble length and the region of interest. However, for better results we suggest that the vibrating crystal frequency be aligned with one of the frequency resolution points for easy identification of the catheter signal, as formulated in Equation 8.

Limiting the region of interest for locating the catheter tip will support a higher frame rate in conventional ultrasound machines.

The blood flow velocity for cardiac applications can go up to 100 cm/s which correspond to frequencies up to 3 kHz. However conventional pulse wave Doppler is usually limited to pulse repetition frequency of 3 kHz, which implies detection of frequencies up to 1.5 kHz. A continuous wave Doppler is used to estimate velocities with frequency greater than 1.5 kHz but is limited to a gated region which is usually a few A lines. Pulse wave Doppler can be still used to visualize the crystal, however it will appear as zero mean noise as the positive and negative shifts will cancel each other. Even this effect would be limited until the blood flow frequency overwhelms the zero mean noise from the symmetric Doppler shift.

B. Limitations

It is important to note that a 5-MHz linear array transducer was used to demonstrate the agreement between the theoretical development and the basic experimental results. After all, 5-MHz center frequency transducers are commonly used in pediatric applications. Clinical ultrasound systems used for adult Doppler imaging usually operate at lower center frequencies, typically around 1 to 3 MHz.

The results reported in this study were obtained in a flow phantom with stationary objects and under undisturbed ultrasound transmit conditions. One would expect to observe some level of artifacts due to physiological motion during in vivo application of this method. While the frequency range of physiological motion is well below 1 kHz and the piezoelectric crystal vibration is 3 kHz, we expect to observe some reduction in performance. A better understanding of these limitations and system modification required to circumvent them will require in vivo animal studies.

A continuous flow pump was used in this study, whereas a pulsatile flow pump would represent the real-life situation. A pulsatile flow would have various frequency components for blood flow, some of which will interfere with the catheter signal. Taking that into account, we made our algorithm robust for a range of blood flow velocity varying from 0 to 90 cm/s, representing a wide spectrum of frequencies. Experiments using a pulsatile flow phantom and the localization accuracy presented here cannot incorporate all possible confounding variables present during a clinical study. Those may include a restricted scan window between ribs; attenuation, reflection, and refraction imaging artifacts; and possibly suboptimal 2D B-mode scan quality, which may make it difficult to initially identify the catheter within the left ventricle cavity. These limitations should be addressed in future closed-chest animal studies or, ultimately, by trials in humans once appropriate clearance is available.

The piezoelectric crystal used in this application has a resonance frequency of 1.2 MHz, but its role is to produce a Doppler shift in the order of kHz. The choice of 3 kHz ensures that the shifted signal lays within the Doppler bandwidth in the current study. In our future work, we intend to explore the tradeoffs between increasing excitation frequency and reducing the voltage required to excite the crystal. Reducing the crystal excitation frequency to decrease the Doppler pulse repetition frequency or to achieve multiple Doppler shift harmonics is not

advantageous due to the required higher input voltage to excite the crystal at lower frequencies for *in-vivo* applications.

CONCLUSION

We elucidated the physical principles of a Doppler shift produced by the interaction between an actively vibrating piezoelectric crystal and an incident Doppler ultrasound signal. We have developed a catheter with a tip that is acoustically active and unambiguously identified by a PW Doppler using the proposed algorithm and can be visualized by a unique color overlay in real time. The ability to identify the catheter tip in real time can be conducive to ultrasound-guided biopsies and minimally invasive procedures. These studies provide a firm basis for further development of our ultrasound guidance approach for future in vivo applications.

Supplementary Material

Refer to Web version on PubMed Central for supplementary material.

Acknowledgments

Research reported in this paper was supported by the National Institute of Biomedical Imaging and Bioengineering of the National Institutes of Health under the award number R01EB019947.

References

1. Janosi RA, Kahlert P, Plicht B, Bose D, Wendt D, Thielmann M, et al. Guidance of percutaneous transcatheter aortic valve implantation by real-time three-dimensional transesophageal echocardiography--A single-center experience. Minimally Invasive Therapy & Allied Technologies. 2009; 18:142–8. [PubMed: 19431067]
2. Bogunovic N, Faber L, Scholtz W, Mellwig KP, Horstkotte D, van Buuren F. Real-time three-dimensional transoesophageal echocardiography during percutaneous transcatheter occlusion of mitral periprosthetic paravalvular leak. European Journal of Echocardiography. Mar.2011 12:E27. [PubMed: 21239451]
3. Sinha A, Nanda NC, Misra V, Khanna D, Dod HS, Vengala S, et al. Live three-dimensional transthoracic echocardiographic assessment of transcatheter closure of atrial septal defect and patent foramen ovale. Echocardiography. Nov.2004 21:749–53. [PubMed: 15546377]
4. Reading C, Charboneau J, Felmlee JP, James E. US-guided percutaneous biopsy: use of a screw biopsy stylet to aid needle detection. Radiology. 1987; 163:280–281. [PubMed: 3547495]
5. McMahon EM, Jiamsripong P, Katayama M, Chaliki HP, Fatemi M, Belohlavek M. Accurate guidance of a catheter by ultrasound imaging and identification of a catheter tip by pulsed-wave Doppler. Pacing and Clinical Electrophysiology. Jan.2012 35:44–50. [PubMed: 22054263]
6. Landzberg JS, Franklin JO, Langberg JJ, Herre JM, Scheinman MM, Schiller NB. The transponder system: a new method of precise catheter placement in the right atrium under echocardiographic guidance. Journal of the American College of Cardiology. Sep.1988 12:753–6. [PubMed: 3403836]
7. Ben-Haim SA, Osadchy D, Schuster I, Gepstein L, Hayam G, Josephson ME. Nonfluoroscopic, in vivo navigation and mapping technology. Nature Medicine. Dec.1996 2:1393–5.
8. Gyongyosi M, Dib N. Diagnostic and prognostic value of 3D NOGA mapping in ischemic heart disease. Nature Reviews Cardiology. Jul.2011 8:393–404. [PubMed: 21587214]
9. Van Langenhove G, Hamburger JN, Smits PC, Albertal M, Onderwater E, Kay IP, et al. Evaluation of left ventricular volumes and ejection fraction with a nonfluoroscopic endoventricular three-dimensional mapping technique. American Heart Journal. Oct.2000 140:596–602. [PubMed: 11011332]

10. Vilkomerson D, Lyons D. A system for ultrasonic beacon-guidance of catheters and other minimally-invasive medical devices. IEEE Trans Ultrason Ferroelectr Freq Control. 1997; 44:496–504. [PubMed: 18244147]
11. Armstrong G, Cardon L, Vilkomerson D, Lipson D, Wong J, Rodriguez LL, et al. Localization of needle tip with color doppler during pericardiocentesis: In vitro validation and initial clinical application. Journal of the American Society of Echocardiography : official publication of the American Society of Echocardiography. Jan.2001 14:29–37. [PubMed: 11174431]
12. Censor D. Scattering by time varying obstacles. Journal of Sound and Vibration. 1972; 25:101–110.
13. Censor D. Harmonic and transient scattering from time varying obstacles. Journal of the Acoustical Society of America. 1984; 76:1527–1534.
14. Censor D, Newhouse VL, Vontz T, Ortega HV. Theory of ultrasound Doppler-spectra velocimetry for arbitrary beam and flow configurations. IEEE Transactions on Biomedical Engineering. Sep. 1988 35:740–51. [PubMed: 3169826]
15. Mujica N, Wunenburger R, Fauve S. Scattering of sound by sound in the vicinity of the liquid-vapor critical point. Physical Review Letters. Jun 13.2003 90:234301. [PubMed: 12857261]
16. Mujica N, Wunenburger R, Fauve S. Scattering of a sound wave by a vibrating surface. European Physical Journal B - Condensed Matter and Complex Systems. 2003; 33:209–213.
17. Wunenburger R, Mujica N, Fauve S. Experimental study of the Doppler shift generated by a vibrating scatterer. Journal of the Acoustical Society of America. Feb.2004 115:507–14. [PubMed: 15000163]
18. Grant EG, Benson CB, Moneta GL, Alexandrov AV, Baker JD, Bluth EI, et al. Carotid Artery Stenosis: Gray-Scale and Doppler US Diagnosis—Society of Radiologists in Ultrasound Consensus Conference 1. Radiology. 2003; 229:340–346. [PubMed: 14500855]

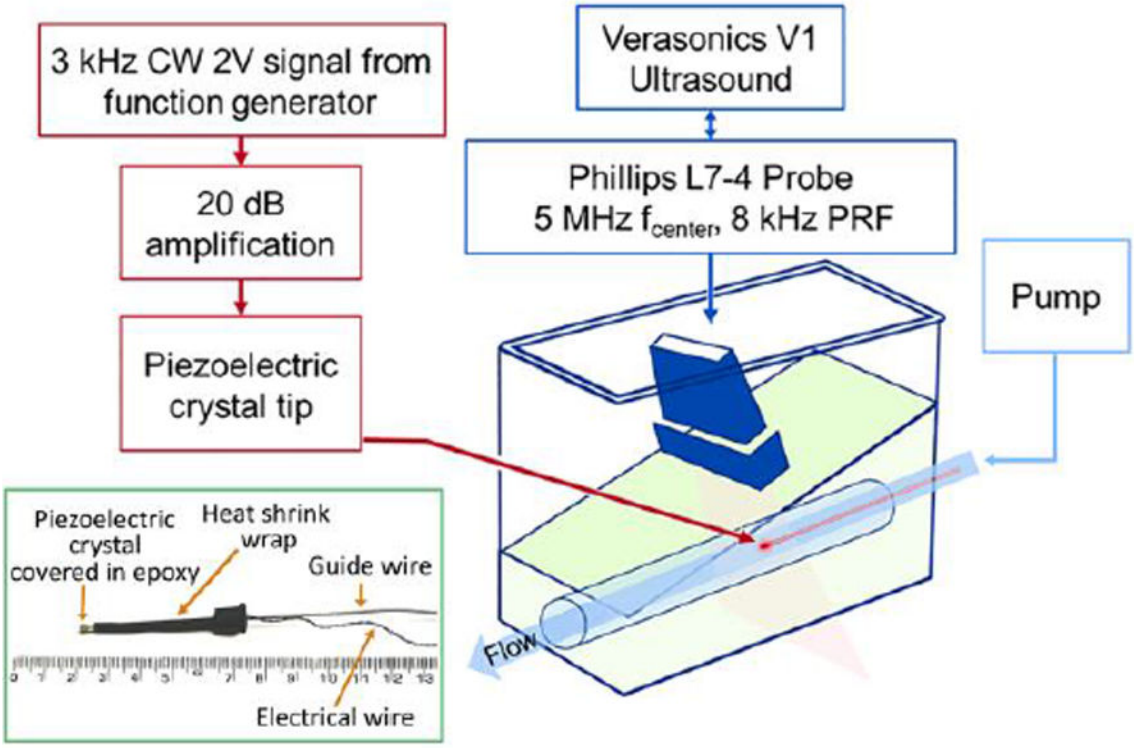

Figure 1.

Setup for testing the proposed algorithm in a continuous flow phantom. PRF indicates pulse repetition frequency. The inset shows the piezo-electric crystal wrapped in heat shrink wrap along with the Guide wire and electrical wire.

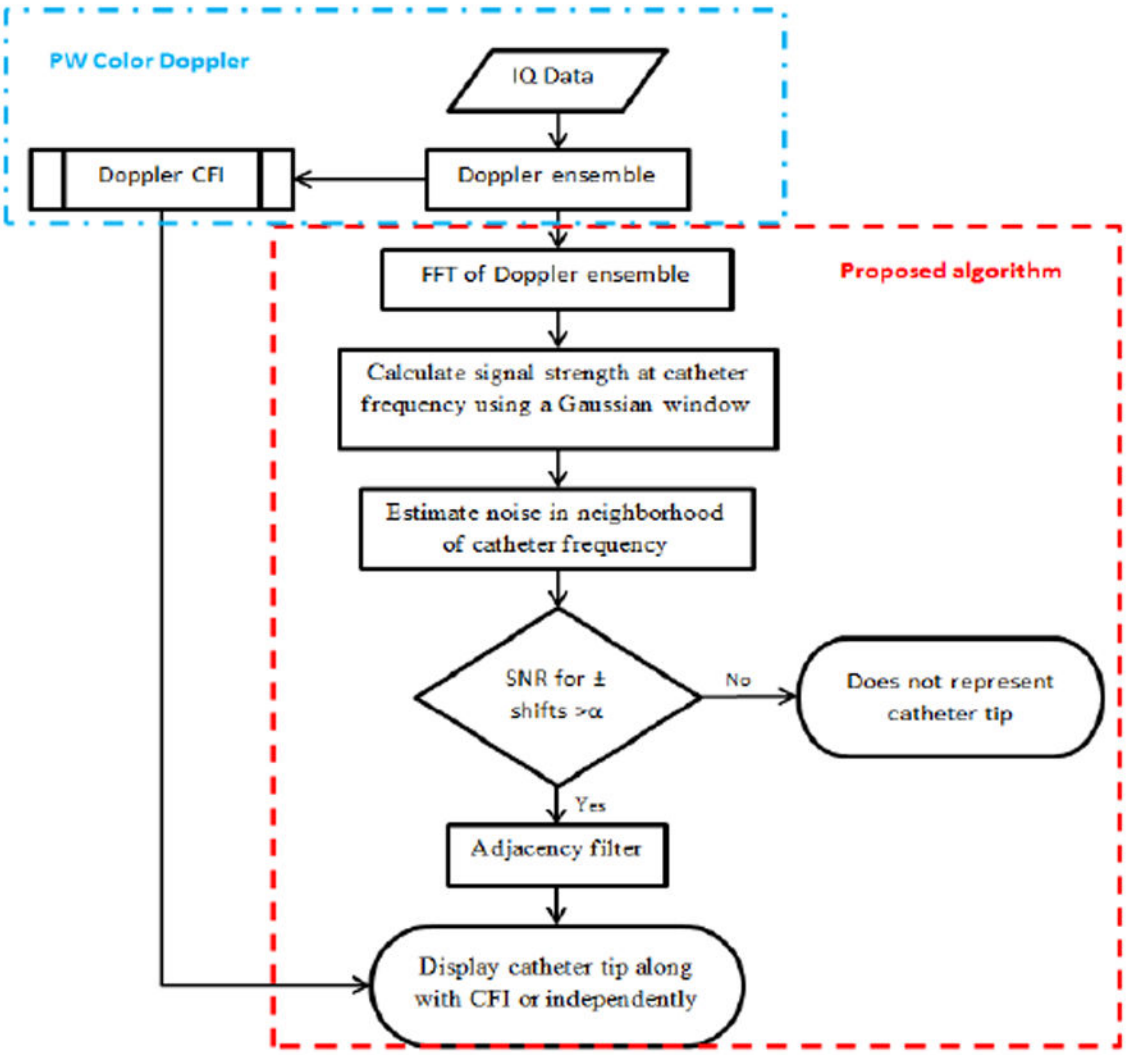

Figure 2.

Flowchart for the proposed algorithm. CFI indicates color flow imaging; FFT indicates fast Fourier transform; IQ indicates in phase quadrature; PW indicates pulse wave; SNR indicates signal to noise ratio.

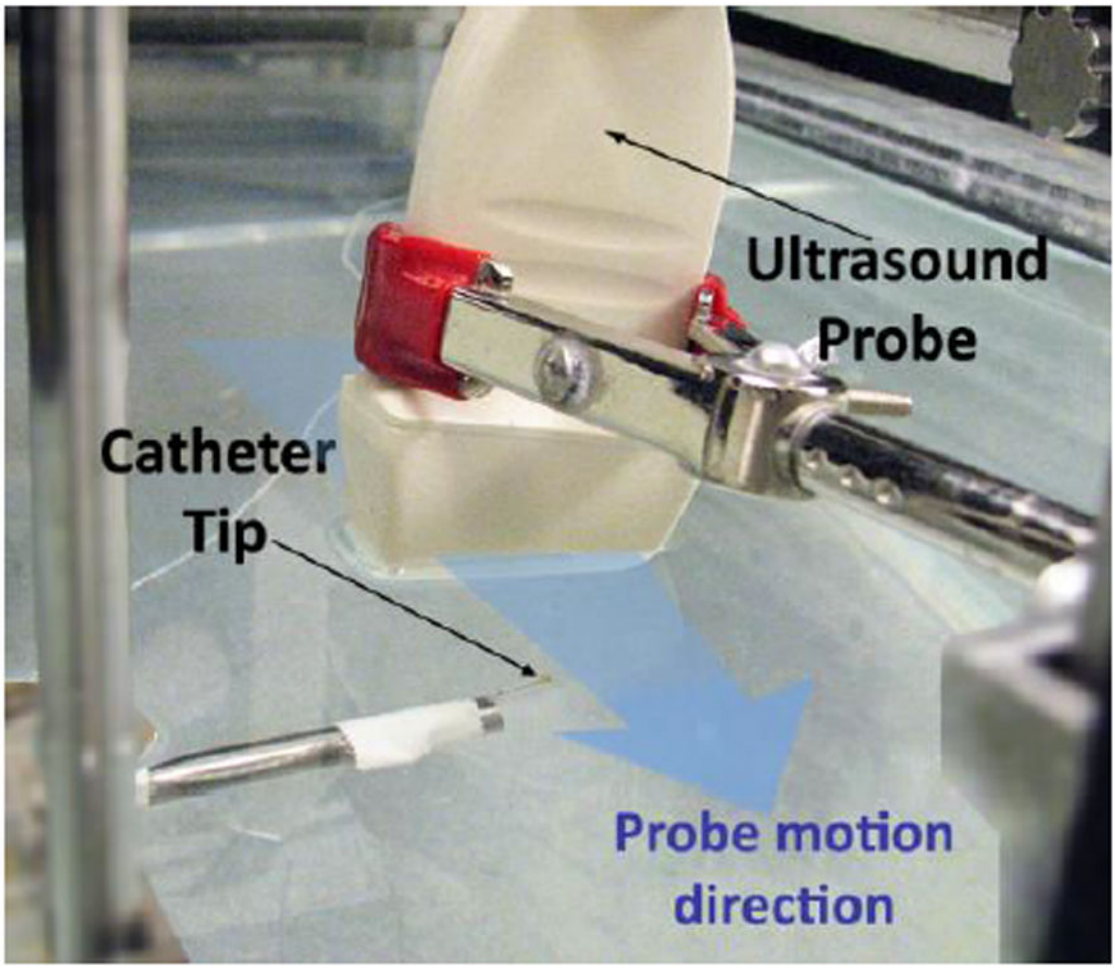

Figure 3.
Experimental setup for localization accuracy of the catheter tip. The linear array transducer is moved in elevational direction over a distance of 4.2 mm in steps of 0.3 mm.

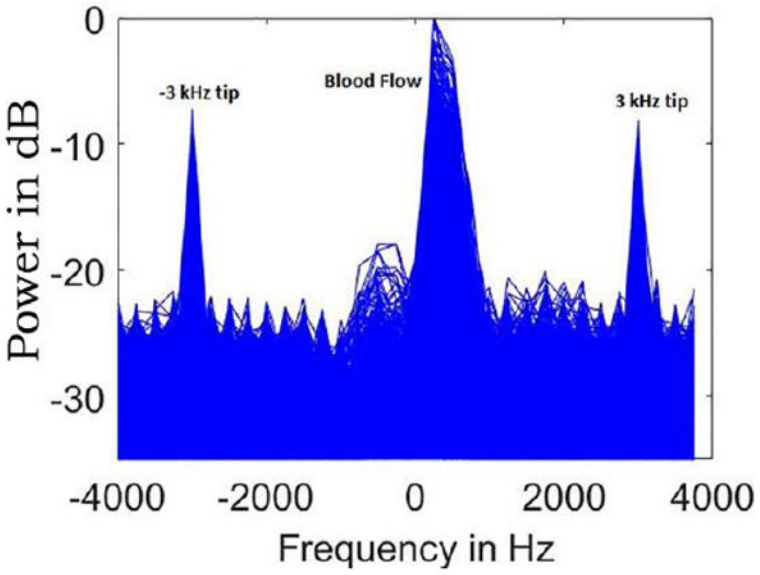

Figure 4.

Spectral power density of a Doppler signal with symmetric positive and negative shifts from the vibrating catheter tip. The signal strength of the blood flow is kept higher than the catheter tip to create a challenging case for testing of the proposed algorithm.

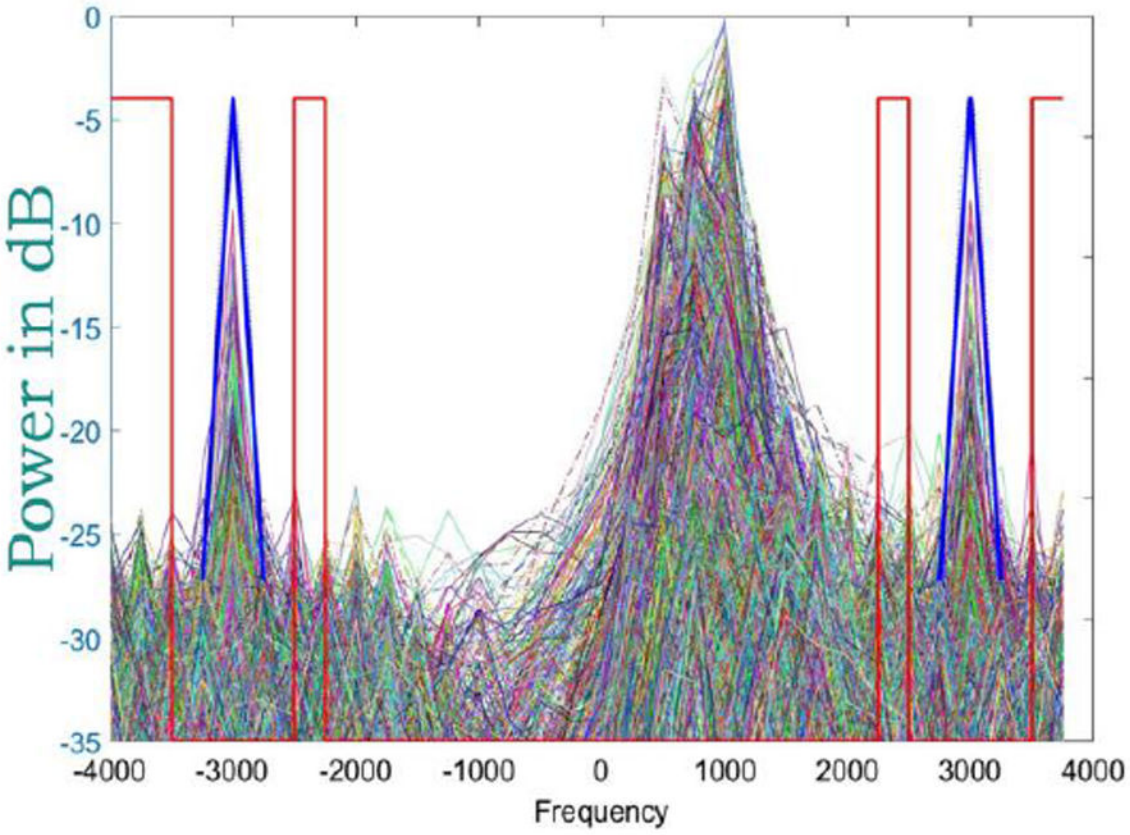

Figure 5.

The estimation of the catheter signal with a Gaussian window (represented in blue) and noise estimation region around the neighborhood of catheter frequency (represented in red).

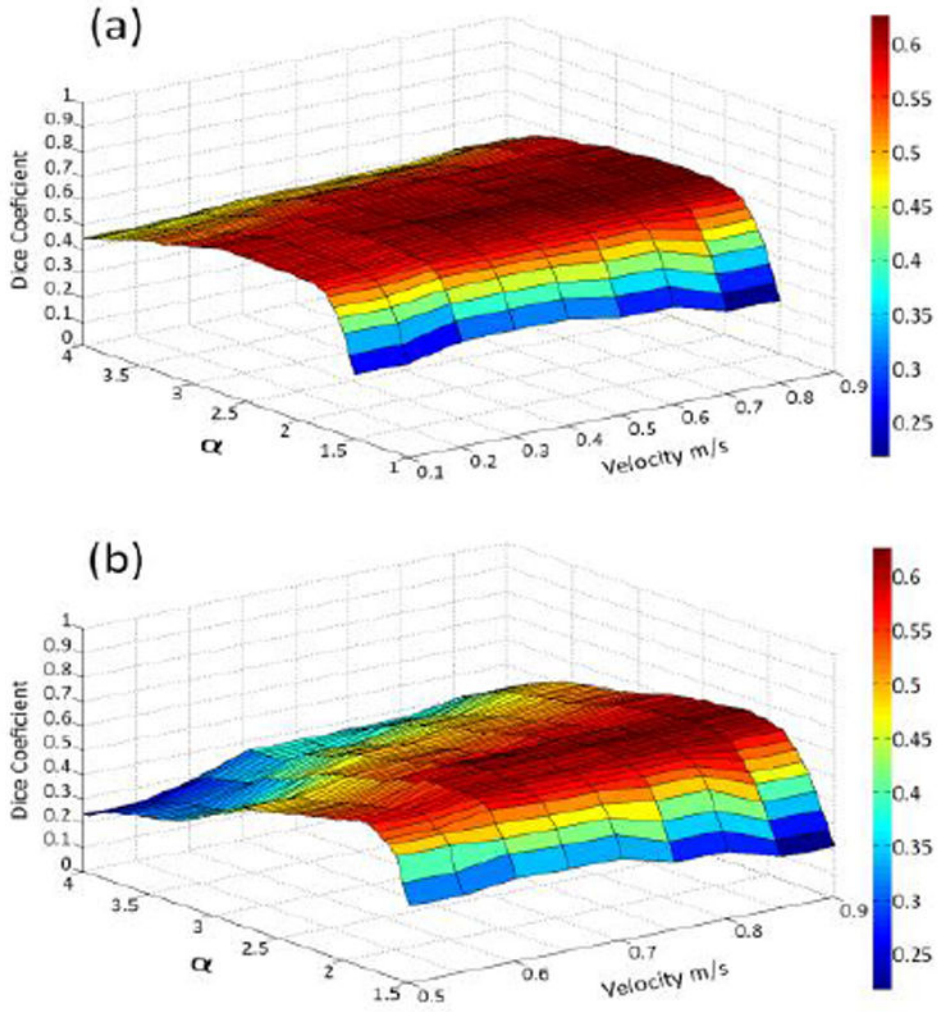

Figure 6.
Threshold cutoff results for (a) velocity 10 to 90 cm/s and (b) high velocity only from 50 to 90 cm/s.

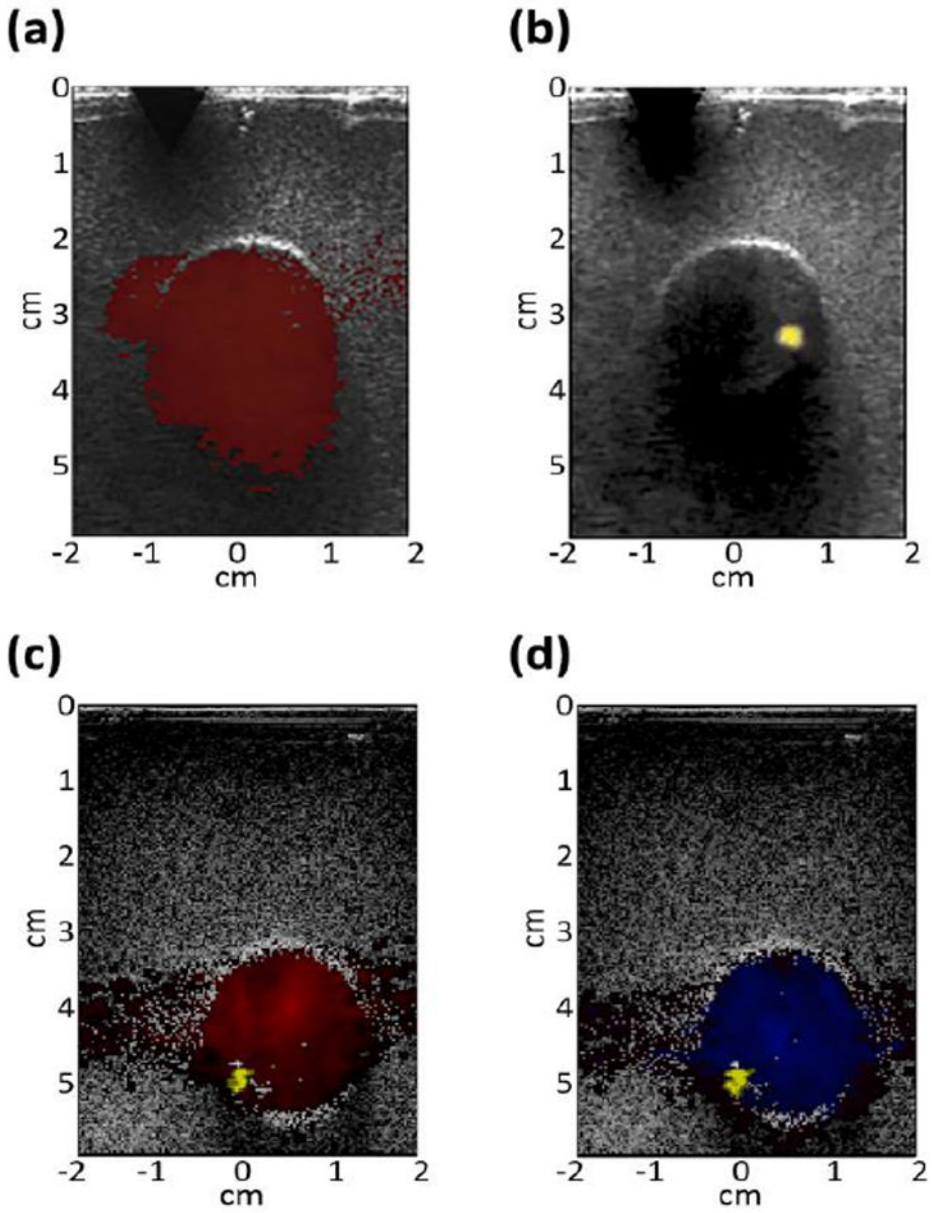

Figure 7.

Ultrasound imaging plane showing (a) Doppler color flow map and (b) catheter tip. (c) Integrated display with Doppler color flow map and catheter tip overlaid on each other. (d) Integrated display with reversed Doppler color flow. Catheter position has changed between (b) and (c), as the crystal was removed and reinserted.

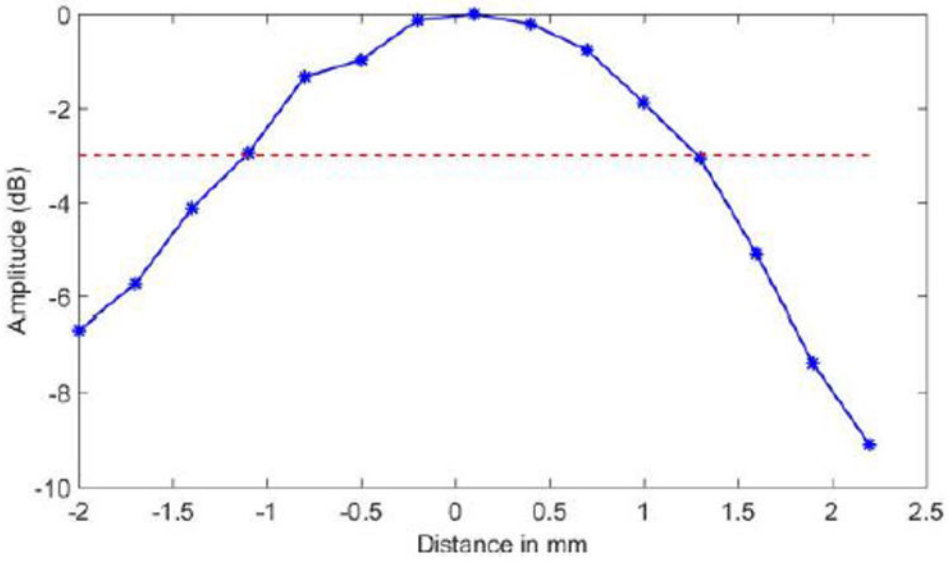

Figure 8.

Amplitude of Doppler sideband as the linear transducer is translated in elevational direction. The red line depicts an amplitude signal of –3dB.